nature communications

Article

https://doi.org/10.1038/s41467-025-57152-7

Cryo-EM structure of the β-1,3-glucan synthase FKS1-Rho1 complex

Received: 27 August 2024

Accepted: 12 February 2025

Published online: 28 February 2025

Check for updates

Jialu Li[1,7], Huayi Liu[2,3,7], Jian Li[2,3,7], Juxiu Liu[1,7], Xinli Dai[1], Angqi Zhu[4], Qingjie Xiao[5], Wenyu Qian[1], Honghao Li[2,3], Li Guo[1], Chuangye Yan[4], Dong Deng[1,6] ✉, Yunzi Luo[2,3] ✉ & Xiang Wang[1,6] ✉

β-1,3 Glucan synthase (GS) is essential for fungal cell wall biosynthesis. The GS holoenzyme comprises the glycosyltransferase FKS1 and its regulatory factor Rho1, a small GTPase. However, the mechanism by which Rho1 activates FKS1 in a GTP-dependent manner remains unclear. Here, we present two cryo-EM structures of FKS1, apo and in complex with Rho1. FKS1 adopts a cellulose synthase-like conformation. The interaction between Rho1 and FKS1 is enhanced in the presence of GTPγS. Rho1 is positioned within a pocket between the glycosyltransferase domain of FKS1 (GT domain) and the transmembrane helix spanning TM7-15. Comparison of the two structures reveals extensive conformational changes within FKS1. These alterations suggest that Rho1's GTP/GDP cycling may act as a molecular pump, promoting a dynamic transition between the resting and active states of FKS1. Notably, Rho1 triggers FKS1 conformational changes that may push the growing glucan chain into FKS1's transmembrane channel, thereby facilitating β-1,3-glucan elongation.

β-1,3-Glucan is an essential component for maintaining fungal cell wall homeostasis[1]. β-1,3-Glucan synthase (GS) plays a pivotal role in cell wall construction through the synthesis of β-1,3-glucan[2]. Owing to its absence in human cells and its widespread distribution in the fungal kingdom, β-1,3-glucan synthase (GS) is a well-established target for antifungal drugs, including echinocandins and ibrexafungerp[3–7].

Numerous previous investigations have consistently demonstrated the multicomponent nature of GS across several fungal species[8–12]. The machinery of GS comprises two essential fractions, Fraction A and Fraction B, both of which are derived from the cell membrane. Combined with and stimulated by GTP, these components collectively govern the full catalytic activity of GS[13,14] (Fig. 1a). The first core component of GS, FKS1 (FK506 supersensitive), which originated from Fraction B, was identified more than three decades ago by several independent groups[11,15,16]. FKS1 is the catalytic subunit of GS and is highly conserved across fungal species. Deletion of FKS1 induces a significant reduction in the β-glucan content within the fungal cell wall, coupled with a concomitant increase in the contents of chitin and mannoprotein constituents[17,18]. Notably, the concurrent disruption of both FKS1 and its paralog FKS2 results in a lethal phenotype in *Candida glabrata* and *Saccharomyces cerevisiae*, highlighting the critical importance of these genes in fungal viability[19,20]. Recently, both yeast FKS1 and an echinocandin-resistant mutant FKS1 (S643P) have been structurally characterized by independent research groups, shedding light on putative active sites and sugar channels[21,22]. In addition, Rho1, sourced from Fraction A, serves as an essential regulatory component of GS, marking a crucial milestone in understanding fungal cell wall

[1]Department of Obstetrics, Key Laboratory of Birth Defects and Related Disease of Women and Children of MOE, State Key Laboratory of Biotherapy, West China Second Hospital, Sichuan University, Chengdu, China. [2]Frontiers Science Center for Synthetic Biology (Ministry of Education), School of Chemical Engineering and Technology, Tianjin University, Tianjin 300072, China. [3]State Key Laboratory of Synthetic Biology, Tianjin University, Tianjin 300072, China. [4]State Key Laboratory of Membrane Biology, Beijing Frontier Research Center for Biological Structure, Tsinghua-Peking Joint Center for Life Sciences, School of Life Sciences, Tsinghua University, Beijing, China. [5]Shanghai Synchrotron Radiation Facility, Shanghai Advanced Research Institute, Chinese Academy of Sciences, Shanghai 201204, China. [6]NHC Key Laboratory of Chronobiology, Development and Related Diseases of Women and Children Key Laboratory of Sichuan Province, Sichuan University, Chengdu, China. [7]These authors contributed equally: Jialu Li, Huayi Liu, Jian Li, and Juxiu Liu.
✉e-mail: dengd@scu.edu.cn; yunzi.luo@tju.edu.cn; xiangwang@scu.edu.cn

https://doi.org/10.1038/s41467-025-57152-7

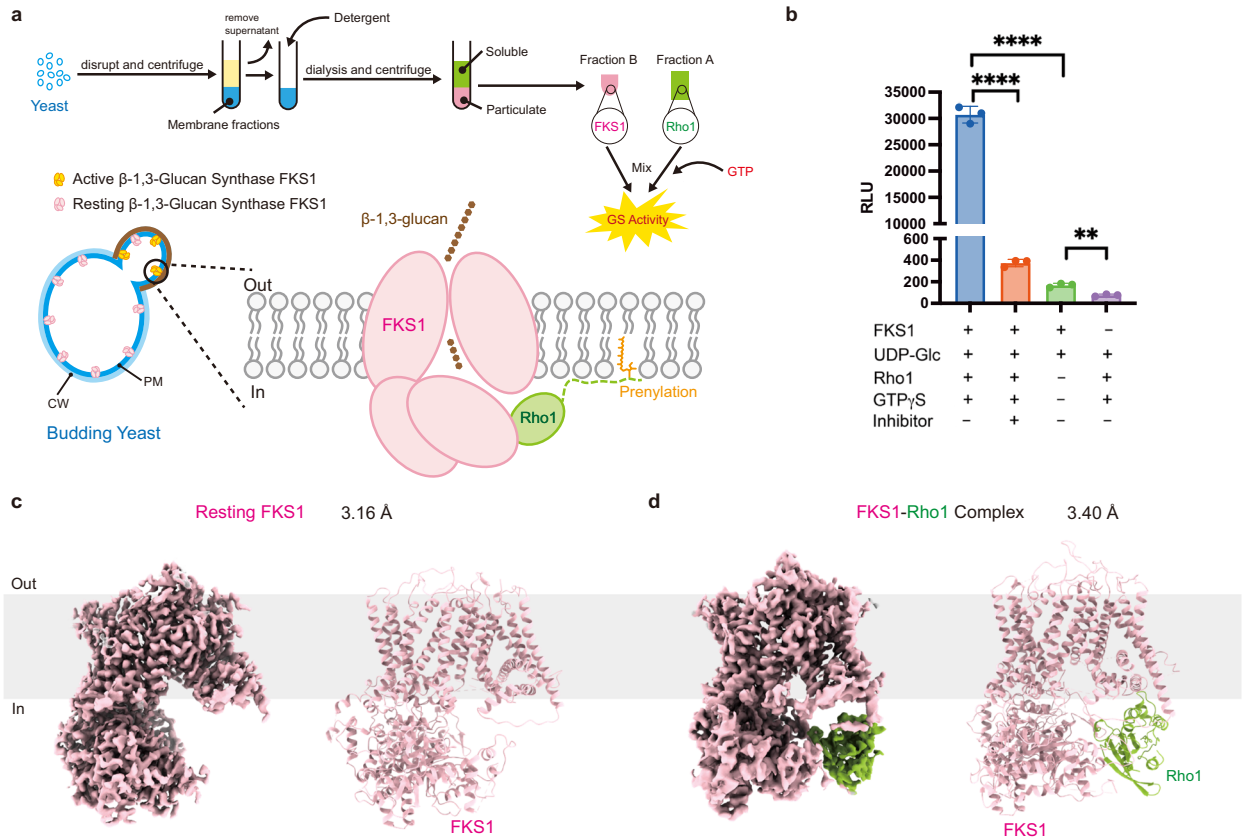

Fig. 1 | Function and cryo-EM structures of *Saccharomyces cerevisiae* FKS1. **a** Schematic diagram of the previously proposed model for FKS1 and Rho1 extraction and purification in β-1,3-glucan synthase. **b** In vitro activity of purified FKS1 in the presence of various effectors, including 0.1 μM FKS1 protein, UDP-Glc (400 μM), Rho1 (1 μM), GTPγS (10 μM), and the inhibitor caspofungin (100 μM), was assessed by monitoring the generated UDP. Data are presented as the mean ± s.e.m. from three independent experiments ($n = 3$). *P*-values determined by two-tailed unpaired *T*-test. $^{**}P < 0.01$, $^{****}P < 0.0001$. Source data are provided as a Source Data file. RLU = relative light units. **c** Overall EM density map and structure of FKS1 in the resting state at 3.16 Å resolution. The FKS1 model and map are colored light pink. All structures are shown as cartoons. **d** Overall EM density map and structure of FKS1-Rho1 complex at 3.40 Å resolution. FKS1 and Rho1 are colored light pink and olive green, respectively.

synthesis[13,14]. However, the precise molecular basis of Rho1-mediated FKS1 activation remains unknown, primarily due to the lack of structural information on the FKS1-Rho1 complex.

Here, we report the cryo-EM structures of FKS1 in both the resting and active states. Our structural analysis and mutagenesis studies provide a comprehensive view of the fully active GS structure in β-1,3-glucan biosynthesis.

Results

Characterization of *fks1*

There are three *fks* genes in *S. cerevisiae*, namely, *fks1, fks2*, and *fks3*, that encode the catalytic subunit of GS[5]. To confirm the predominant gene, we employed the CRISPR-Cas9 system for single and double knockout of the yeast *fks* genes (Supplementary Fig. 1a). In agreement with the findings of a previous study, the generation of a double knockout strain of *fks1* and *fks2* was unsuccessful, resulting in lethality[19]. Deletion of *fks1* altered the composition of the yeast cell wall, especially the glucose-to-mannose ratio (Supplementary Fig. 1a). A comparison of the cell wall composition of yeast revealed that the wild-type strain presented an approximate glucose-to-mannose ratio of 1 within the cell wall components, which is consistent with prior reports[17,18]. The *fks1* deletion strains presented a ratio of ~0.5, in contrast with the other knockout strains, which exhibited no significant difference in the glucose-to-mannose ratio (Supplementary Fig. 1a and Fig. 12). These findings highlight the pivotal role of *fks1* in cell wall synthesis.

Structure determination of FKS1

To obtain functional FKS proteins, we generated a yeast strain (BY4741-FSH) with C-terminal tags appended to the three *fks* genes: a Flag tag for FKS1, a Strep tag for FKS2, and a His tag for FKS3. Full-length FKS1 was purified to homogeneity from this yeast strain. In size-exclusion chromatography (SEC) experiments, FKS1 was eluted at 14.3 ml with a monodisperse peak (Supplementary Fig. 1b). The homogeneous Rho1 protein was expressed and purified from insect cells (Supplementary Fig. 1c).

We subsequently assessed the activity of the purified FKS1 protein by using the UDP-Glo glycosyltransferase assay, a well-established method for determining glucan synthase activity[21,22] (Fig. 1b). FKS1 alone exhibited minimal weak activity, but its activity was highly enhanced upon the addition of Rho1 and guanosine 5′-O-(3′-thiotriphosphate) (GTPγS) (Fig. 1b). Furthermore, caspofungin, a representative echinocandin drug, effectively inhibited FKS1 activity (Fig. 1b). In addition, FKS1 catalyzed the conversion of UDP-glucose into a water-insoluble polymer in the presence of Rho1 and GTPγS. This polymer was specifically stained by aniline blue and can be hydrolyzed by endo-1,3-β-glucanase, consistent with previous study[21] (Supplementary Fig. 13). These results confirm the successful preparation of functional FKS1 and Rho1 proteins for further structural studies.

The functional and biochemical studies described above have provided a strong foundation for uncovering previously uncharacterized GS conformations and advancing our understanding of the complete activation and regulatory mechanisms of GS. Here, we solved

https://doi.org/10.1038/s41467-025-57152-7

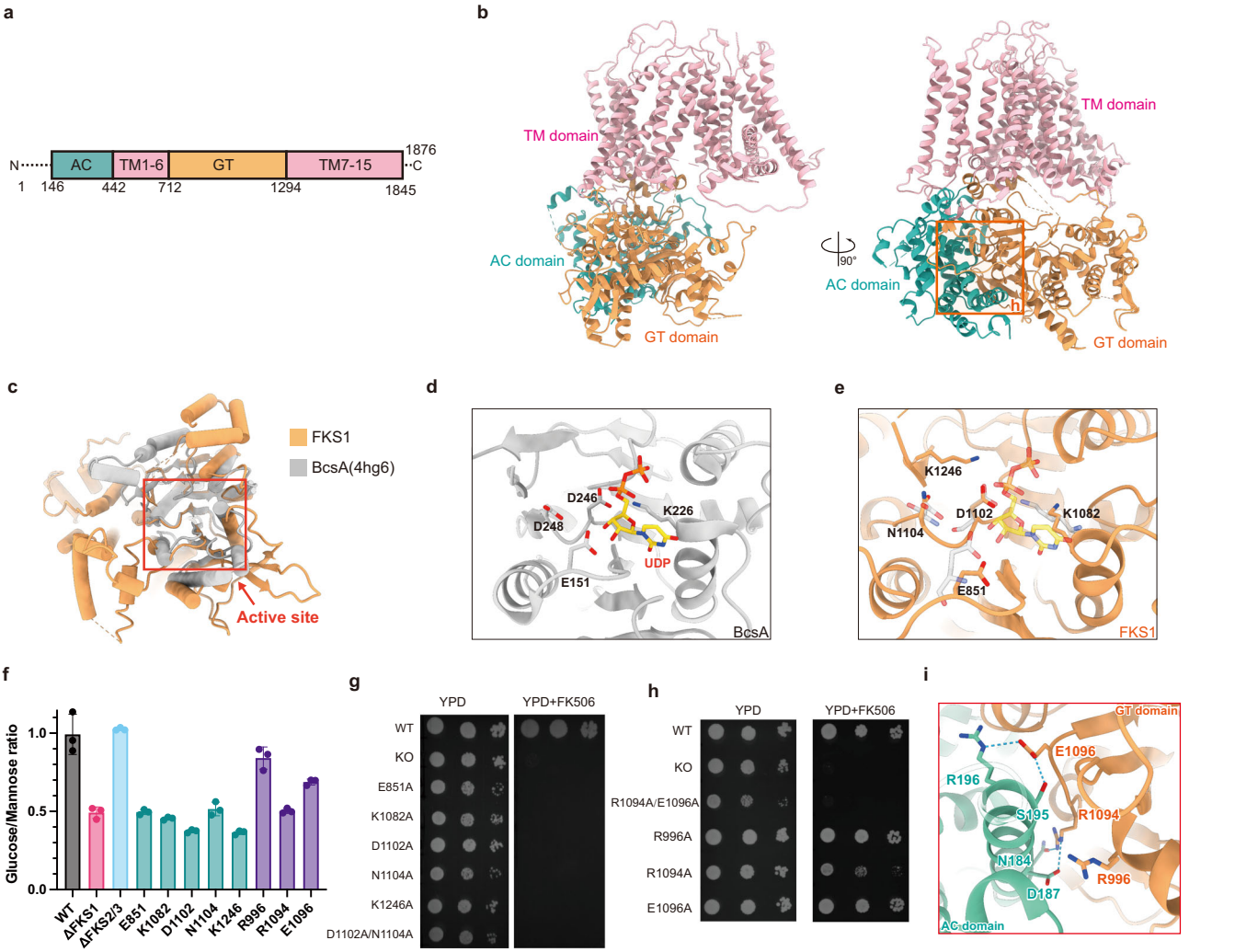

Fig. 2 | The active site and domain interaction of FKS1. a Domain architecture of FKS1. Schematic representation displaying the transmembrane (TM), accessory domain (AC), and glycosyltransferase (GT) domains. **b** Overall structure of FKS1 in the apo state. The TM domain, AC domain, and GT domain of FKS1 are colored light pink, medium aquamarine, and orange, respectively. **c** Superposition of the GT domain of FKS1 (colored in orange) and BcsA (PDB code: 4hg6, shown in grey). **d** Close-up view of the BcsA active site with UDP and key residues involved in substrate binding highlighted as sticks. **e** Close-up view of the FKS1 active site with key residues highlighted as sticks. Transparent sticks show corresponding residues and UDP from BcsA for comparison. **f** Proportion of glucose and mannose in the cell wall of wild-type and different FKS1 active site mutation strains. Data are presented as the mean ± s.d. from three independent biological replicates ($n = 3$). Source data are provided as a Source Data file. **g** In vivo functional assay of active site mutations in FKS1. The growth of mutant strains was assessed on YPD plates without (left panel) and with (right panel) the FKS2 transcriptional regulator FK506, a calcineurin inhibitor that inhibits FKS2's expression. **h** In vivo functional assay of AC and GT domain interaction mutations in FKS1. The growth of mutant strains was assessed on YPD plates without (left panel) and with (right panel) the FKS2 transcriptional regulator FK506. **i** Domain interaction of AC domain and GT domain of FKS1. The AC domain and GT domain of FKS1 are colored medium aquamarine and orange, respectively. The key residues of domain interaction are show as sticks.

the cryo-EM structures of FKS1 at a resolution of 3.16 Å and the FKS1-Rho1 complex at 3.4 Å (Fig. 1c, d and Supplementary Table 1). These density maps facilitated the construction of an atomic model of FKS1 and delineated the assembly of the FKS1-Rho1 complex.

Overall structure of FKS1

In the context of Carbohydrate-Active Enzymes (CAZy) classification, FKS1 is categorized within the GT48 family of GT-A–type glycosyltransferases (GTs). We performed cryo-EM on FKS1, which comprises 15 transmembrane helices (TMs) and a large cytoplasmic domain (Fig. 1c and Supplementary Fig. 4a). Specifically, the cytosolic region consists of an N-terminal domain known as the accessory domain[21] (AC domain, residues 146-442) and a GT domain (residues 712-1294) (Fig. 2a). Despite differences in the detergents used for FKS1 purification, our FKS1 structure is similar to previously elucidated FKS1 structures[21]. Structural superimposition with the reported FKS1 structure (PDB: 7xe4) was achieved, with a root-mean-square-deviation (RMSD) value of 1.1 Å over 1489 residues (Fig. 2b and Supplementary Fig. 3a). In accordance with the weak activity observed for FKS1 alone, our FKS1 structure likely represents a resting state, offering a detailed view of the enzyme architecture before Rho1 increases its activity.

Notably, a homologous structure search with the Dali server[23] and Foldseek[24] revealed that the GT domain of FKS1 shares a similar catalytic fold with that of the bacterial cellulose synthase BcsA[25–27]. The putative active site of FKS1 was subsequently proposed, pinpointing functionally critical residues, including E851, K1082, D1102, N1104, and K1246 (Fig. 2c-e). These residues were mutated to alanine via CRISPR at the *fks1* locus, followed by functional characterization involving the measurement of glucose-to-mannose ratios in cell wall glucans and growth phenotype assays in the presence of FK506. All the mutations resulted in reduced mannose-to-glucose ratios relative to the WT

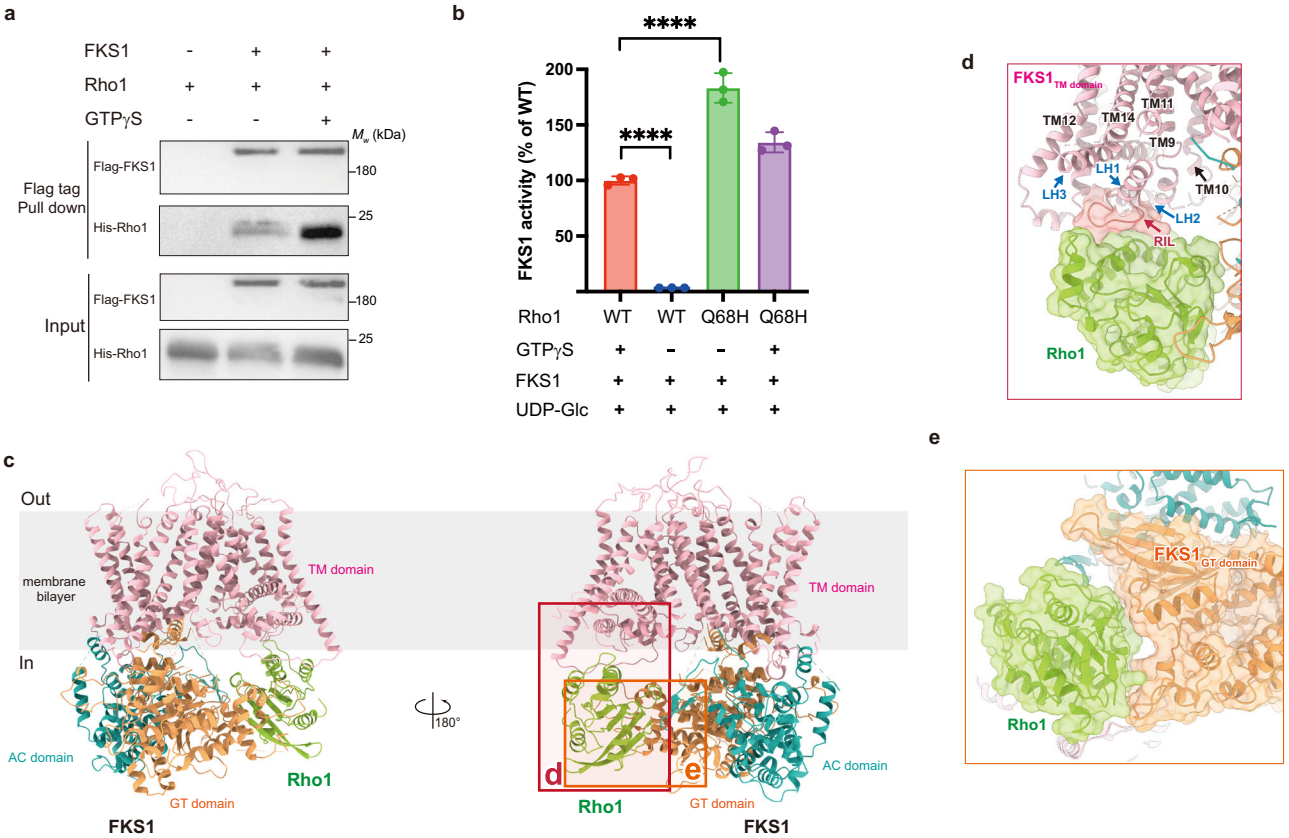

Fig. 3 | Rho1 in the active state promotes the activity of FKS1. a Pulldown assay result indicate the interaction between FKS1 and Rho1 is enhanced by adding GTPγS. Flag-tagged FKS1 was purified and incubated with purified His-tagged Rho1 with or without added GTPγS. The mixture was immunoprecipitated with Flag-tagged FKS1 and immunoblotted with anti-Flag and anti-His antibodies, respectively. Source data are provided as a Source Data file. **b** In vitro activity of purified FKS1 with Rho1 and Rho1^{Q68H}. Activity was measured by monitoring the UDP generated. The reaction mixture contained 0.1 μM FKS1 protein, 400 μM UDP-Glc, and 1 μM Rho1 (or Rho1^{Q68H}), with or without 10 μM GTPγS. Data are presented as the mean ± s.e.m. from three independent experiments ($n = 3$). The activities were normalized against the wild-type (WT) FKS1 protein with UDP-Glc, Rho1, and GTPγS. *P*-values determined by two-tailed unpaired *T*-test. ****$P < 0.0001$. Source data are provided as a Source Data file. **c** Overall structure of the FKS1-Rho1 complex shown in ribbon. The TM domain, AC domain, and GT domain are highlighted by different colors. Rho1 is colored green. **d**, **e** Interactions between Rho1 and FKS1. Surface views of Rho1 and FKS1 are shown as transparent. The RIL (Rho1 interaction loop of FKS1) was colored in red.

strain, indicating the critical role of these sites in FKS1. Notably, the individual mutations E851A, K1082A, and N1104A resulted in slow growth, even in the absence of FK506 (Fig. 2f, g and Supplementary Fig. 3b).

Furthermore, extensive interaction between the AC domain and the GT domain was identified by PDBePISA[28], burying a total interface area of 2371 Å^2 (Supplementary Fig. 8). We characterized several amino acids that are critical for hydrogen bond interactions between AC and the GT domain, such as R996A, R1094A, and E1096A (Fig. 2i). Double mutation (R1094A-E1096A) and single mutation (R1094A) significantly altered the glucose-to-mannose ratios of cell wall composition and substantially reduced the growth rate of strains on FK506-containing plates (Fig. 2h, i). Notably, several point mutations within the AC domain, such as E146V, V302N, R319A, Y329N, and Y335N, have been reported to be temperature sensitive and have significant effects on cell wall components[18,29] (Supplementary Fig. 3c). These results indicate the pivotal role of AC-GT domain interactions in regulating FKS1 activity.

In vitro reconstitution of GS

It is generally believed that Rho1 should interact directly with FKS1[30,31]. Our Flag pulldown and activity assays confirmed the direct interaction between purified FKS1 and Rho1 (Fig. 3a, b). Moreover, GTPγS increased FKS1 and Rho1 binding. Consistently, our activity assays revealed that GS activation also depends on GTPγS (Fig. 3b). Interestingly, a constitutively active Q68H mutation of Rho1 activated FKS1 in a GTPγS-independent manner, which is consistent with results reported in a previous study[13] (Fig. 3b).

Notably, extensive trials to purify endogenous GS complexes have consistently yielded only FKS1, which lacks detectable Rho1. This aligns with the dynamic nature of most Rho-effector interactions, which are often characterized by rapid GTP-dependent association and dissociation[30]. We therefore infer a similar transient interaction between FKS1 and Rho1.

Recognizing the challenges in purifying the endogenous GS complex, we endeavored to reconstitute the GS complex using the purified FKS1 and Rho1 proteins in vitro (Supplementary Fig. 1b, c). Bissulfosuccinimidyl suberate (BS3) crosslinking experiments further validated the direct interaction between Rho1^{Q68H} and FKS1 (Supplementary Fig. 1d-f).

Structure of the FKS1-Rho1 complex

We collected cryo-EM videos of FKS1-Rho1 non-crosslinked samples. During 2D classification, an obvious excess of globular density was observed on the cytoplasmic side in comparison with the individual FKS1 samples (Supplementary Fig. 4). This additional density was weak and ambiguous, which may be attributable to partial dissociation of some FKS1-Rho1 complex particles within the cryo-EM sample. To address this issue, we further prepared BS3-crosslinked FKS1-Rho1^{Q68H} complex samples for cryo-EM data collection. Ultimately, the data

https://doi.org/10.1038/s41467-025-57152-7

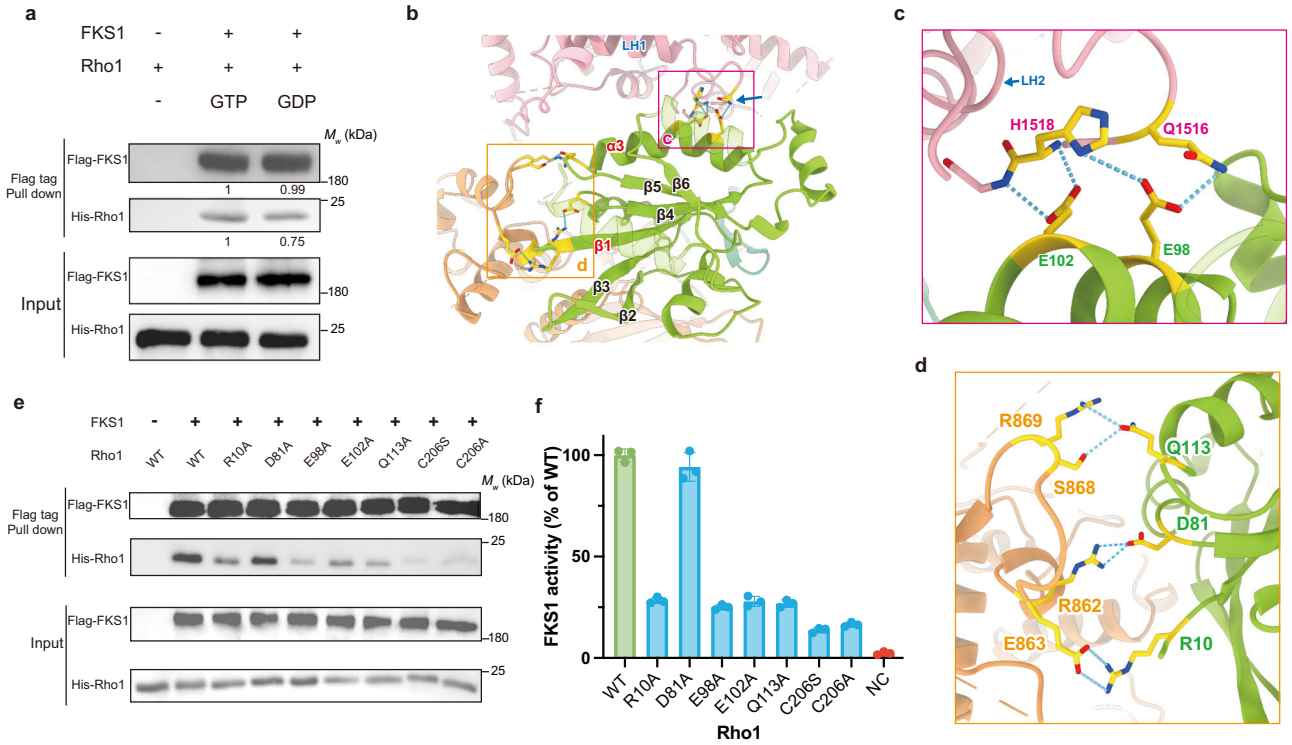

Fig. 4 | Molecular basis for Rho1 binding to FKS1. a Flag pulldown assay of Rho1 and FKS1 in the presence of GTP or GDP. The pulldown assay was independently performed three times and representative results are shown. The relative levels of FKS1 and Rho1 were quantified by ImageJ and shown below the corresponding blots. Source data are provided as a Source Data file. **b** Overview of Rho1-FKS1 Interface. The intermolecular interfaces between Rho1 (green) and the FKS1 GT domain (orange), as well as the RIL loop in FKS1. **c** Close-up view of the interaction between the α3 helix of Rho1 and the Rho1 Interaction Loop (RIL) of FKS1, highlighting key residues involved in binding. **d** Close-up view of the interaction between the GT domains of Rho1 and FKS1. **e** Flag pulldown assay to assess the binding of wild-type (WT) Rho1 and various mutations to FKS1. Source data are provided as a Source Data file. **f** In vitro glycosyltransferase activity of Rho1 mutants. Enzyme activity assay to evaluate the impact of Rho1 mutations on FKS1's glycosyltransferase activity. Data are presented as the mean ± s.e.m. from three independent experiments ($n = 3$). Source data are provided as a Source Data file.

provided a density with a resolution of 3.40 Å, which enabled us to build an accurate model of FKS1 and Rho1, confirming the specific interaction between the two proteins (Supplementary Fig. 5 and Fig. 15).

The cryo-EM structure of the FKS1-Rho1 complex reveals a pronounced wedge-shaped architecture, with the Rho1 monomer positioned within the cytoplasmic cleft of FKS1. Rho1 is positioned between the GT domain and four lateral helices (LH1–4) of FKS1 (Fig. 3c-e). LH1–4 are located on Rho1 (Fig. 3d), and Rho1 neighbors the GT domain (Fig. 3e). Given the crucial function of the GT domain in substrate binding (UDP-glucose) and catalysis, this structural arrangement implies that Rho1 might induce conformational changes in the GT domain.

The globular shape of Rho1^{Q68H} is characterized by a central six-stranded β-sheet surrounded by six helices (Supplementary Fig. 6a and 9). However, the flexible C segment was not visible, likely because of disorder. Extensive conformational switches within the Rho GTPase family are well documented[32], particularly in Switch I and Switch II, upon the transition between the GTP-bound state and GDP-bound state (Supplementary Fig. 6b). In agreement with previous molecular dynamics studies, the constitutively active Rho1^{Q68H} mutation adopts a conformation closely resembling the conformation of the GTP-bound state of Rho1 (Supplementary Fig. 6c). The structure of Rho1 ^{Q68H} bound to FKS1 shows no significant conformational changes compared with previously reported structures of the GTP-bound forms of Rho1[33] (Supplementary Fig. 6c). Moreover, the interaction pattern between the GT domain of FKS1 and Rho1 resembles the binding configuration observed between Sec 3 and Rho1[33] (Supplementary Fig. 6d). Although β-1,3-glucan was not present within the TM domain, the FKS1 and Rho1^{Q68H} complex exhibited full β-1,3-glucan synthase activity independent of GTPγS (Fig. 3b). This finding strongly suggests that the captured FKS1-Rho1 binary complex represents the active state of GS.

Molecular basis for Rho1 binding to FKS1

To explore the impact of GDP/GTP exchange on the interaction between Rho1 and FKS1, we conducted a pulldown assay of FKS1 in the presence of GDP or GTP. Consistent with the results of the GTPγS experiments, the presence of GTP appeared to enhance Rho1 binding to FKS1 compared with that of GDP (Fig. 4a). These results suggest a potential preference for the GTP-bound form of Rho1 in FKS1 binding, which aligns with previous studies demonstrating greater activity in the presence of GTP than in the presence of GDP[13].

The cryo-EM structure of the FKS1-Rho1 complex revealed an extensive interface between Rho1 and FKS1, burying ~571 Å^2 of the hydrophobic surface. Despite the limited local resolution of Rho1, we analyzed the putative FKS1-Rho1 interface. There are two primary binding interfaces of FKS1: one at the expected GT domain interface and another at a loop between LH1 and LH2 (residues 1511-1521, called the Rho1 interaction loop, RIL) (Fig. 4b). The interaction between Rho1 and FKS1 occurs mainly through extensive hydrophilic interactions around α3 helix regions (residues 89-113 for the α3 helix) (Fig. 4b). The α3 helix in Rho1 contacts RIL in FKS1. Detailed quantitative analysis via PDBePISA[28] identified key residues in Rho1's α3 helix (residues E98, E102, and Q113) and RIL in FKS1 (residues Q1516 and H1518) that strongly contributed to this interaction (Fig. 4c). Our structural analysis highlighted the critical role of the α3 helix and N-terminal residues of Rho1 in FKS1 binding. Interestingly, a comparative analysis of human

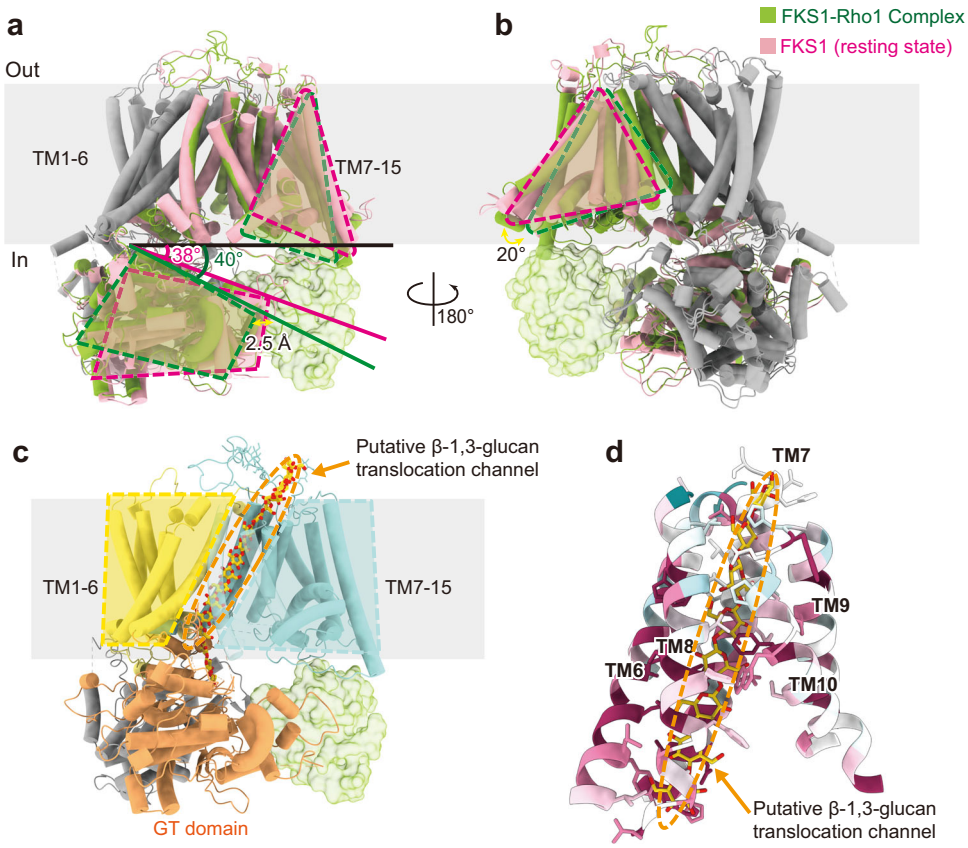

Fig. 5 | The dynamic regulation model of FKS1 in the cell wall synthesis of yeast. **a**, **b** Conformational changes of FKS1 compared with binding Rho1. The structure of Rho1 is shown as surface, and FKS1 is shown as cylinder. The residues 145-712 (colored gray) of apo FKS1 and FKS1-Rho1 complex are superposed, and the remaining parts are colored green and pink, respectively. **c** Putative sugar chain exit channel in FKS1-Rho1 complex compared to BcsA. Only the BcsA sugar chain (gold) is displayed for clarity. **d** The conserved amino acids in TM6, TM8, TM9, and TM10 of FKS1 are proposed to constitute the putative sugar chain exit channel. Conservation analysis was performed using ConSurf (https://consurf.tau.ac.il/consurf_index.php).

RhoA and yeast Rho1 homologs revealed a critical 27-residue segment (mainly the α3 helix) within Rho1. The differences in the α3 helix in Rho A were unable to rescue Rho1 function in previous studies, corroborating its importance as a crucial FKS1-interaction interface[34].

Additionally, residues such as R10 from β1, D81 from the loop between β3 and β4, and switch loop II in Rho1 also contributed to the interaction with FKS1's GT domain (Fig. 4d and Supplementary Fig. 6e). The switch loop II pointed toward the catalytic pocket of FKS1, suggesting the potential influence of these segments on FKS1 activation upon GTP hydrolysis. The Rho1 residues involved in FKS1 binding are highly conserved in human RhoA (90.9% identity for 11 residues). Furthermore, our structural insights into the electrostatic surface potential of Rho1 highlighted its negatively charged nature, suggesting an attractive interaction with the positively charged pocket of FKS1 (Supplementary Fig. 7). This positively charged pocket of FKS1, comprising specific amino acids, including R1508, R1512, R1519, K1636, K1637, and K1788, played a central role in these interactions (Supplementary Fig. 7). Our structural analysis revealed the critical role of charge interactions in this molecular interplay.

Next, we performed a pulldown assay using the FKS1 protein and Rho1 mutant proteins to validate the observed interactions. Consistent with the structural observations, the E98A mutation in the α3 helix largely reduced FKS1 binding, as did the R10A mutation in the N-terminus of Rho1 (Fig. 4e). D81A, E102A and Q113A had modest effects on binding (Fig. 4e). Glycosyltransferase assays further validated these findings; R10A, E98A, E102A and Q113A abolished FKS1 activity (Fig. 4f). In conclusion, our comprehensive structural and mutational analyses revealed the preference of the GTP-bound form of Rho1 for FKS1 binding, elucidating the pivotal roles of interface amino acids and charge interactions in governing the Rho1-FKS1 interaction mechanism.

Activated Rho1 induces a conformational change in FKS1

Upon superimposing the structures of the apo- and Rho1-bound structures of FKS1, large conformational changes were observed in both transmembrane helices TM7-TM15 and the GT domain (Fig. 5a, b). There is a 2.5 Å horizontal translation and 2-degree vertical rotation in the GT domain, which is in line with the 3D variability analysis (Fig. 5a and Supplementary Video. 1). In the FKS1-Rho1 complex, transmembrane helices 7–15 exhibited a notable 20-degree rotation (Fig. 5b). Alignment with cellulose synthase structures revealed the putative channel for sugar chain exit between TM1-6 and TM7-15, suggesting that the rotation of TM7-15 facilitates sugar chain translocation[26,27] (Fig. 5c, d).

Discussion

Our investigation of two distinct structural snapshots of FKS1, coupled with extensive functional characterization, significantly contributes to the mechanistic understanding of fungal cell wall β-1,3-glucan synthesis. In the FKS1 apo state, we discovered that the AC and GT domains form a tight structural unit, emphasizing the vital role of their stable interaction in sustaining FKS1 activity. Additionally, the interplay of the AC domain with the GT domain is similar to that of the PilZ domain in BcsA cellulose synthase, suggesting a potential regulatory role for the AC domain in FKS1 activity[25–27].

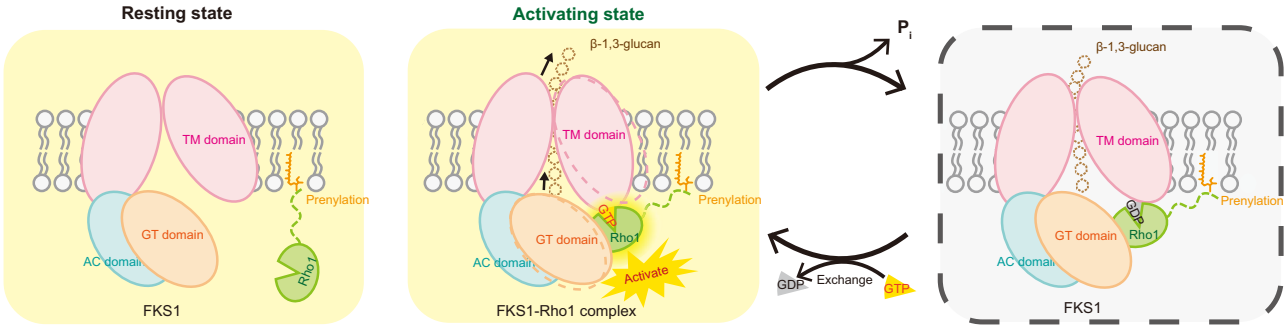

Fig. 6 | Working model for dynamic regulation of FKS1 by Rho1. A proposed ratchet and pawl mechanism for Rho1-mediated activation of FKS1 β-1,3-glucan synthase activity. In left panel, GS remains in a resting state, FKS1 and Rho1 are separated, and the two proteins have not yet enriched or interacted with each other at the site of new cell wall synthesis. In middle panel, GS remains in an activation state upon the GDP/GTP exchange. GTP binding strengthens the interaction between Rho1 and FKS1, triggering conformational changes in both proteins. The FKS1 GT domain and TM7-15 undergo conformational shifts potentially influencing the active site and polymer translocation pathway, thereby pushes the elongated sugar chain out of the membrane channel. After the products UDP and Pi are released, GS returns to the GDP state again. In right panel, Structural interpretation of GS remains in a GDP state. Rho1, bound to GDP, and the α3 helix interacts weakly with RIL loop in FKS1. The FKS1 GT domain and TM7-15 adopt a conformation incompatible with active sugar chain elongation. The nascent sugar chain stalls within the membrane channel formed by TM1-6 and TM7-15. In our model, GTP hydrolysis in Rho1 acts as the "power source" of this cycle. Rho1's GTP-bound state allows "forward" movement of the sugar chain, while the GDP-bound state prevents backward movement.

The pivotal role of Rho1 in regulating fungal β-1,3-glucan synthase (FKS1) activity highlights the importance of elucidating their interaction interface. The FKS1-Rho1^{Q68H} complex elucidates the binding interface for FKS1, where the interaction is largely facilitated by the attraction of opposing surface electrostatic charges. In addition, prenylation at C206 of Rho1 facilitates its anchoring to the yeast cell membrane[35]. Interestingly, alanine or serine substitutions at C206 severely affected Rho1 binding and GS activity (Fig. 4e), implying the presence of additional interaction interfaces in the cell membrane region[21]. The experimentally resolved structure of the FKS1-Rho1 complex differs significantly from the AlphaFold3-predicted model, particularly in the relative positioning of Rho1. In the predicted model, Rho1 is situated laterally, whereas our experimental data indicate that Rho1 is inserted into the catalytic domain of FKS1 (Supplementary Fig. 14). Upon Rho1 binding, we observed a significant conformational change in FKS1, particularly in the TM7-15 and GT domains. These alterations likely facilitate the extension of the sugar chain to push out of the membrane channel of FKS1 (Fig. 6). Inspired by mechanistic insights from the bacterial cellulose synthase BcsA-BcsB complex, we propose a working model for the FKS1-Rho1 complex[27]. This model employs a "ratchet and pawl" mechanism to elucidate the dynamic regulation of FKS1 activity by Rho1. The distinct conformational states of Rho1, influenced by GTP binding and hydrolysis, orchestrate the interaction with FKS1, thereby modulating the enzyme's activity. This mechanism highlights the critical role of Rho1 in controlling FKS1 function while emphasizing the intricate interplay between structural dynamics and enzymatic processes in fungal cell wall synthesis. The ability of Rho1 to switch between active and inactive states serves as a critical regulatory point, ensuring efficient and directional elongation of the β-1,3-glucan polymer (Fig. 6). Despite the absence of the substrate donor UDP in the FKS1 structure, the precise catalytic mechanisms of FKS1, such as glycosyl transfer, polymer translocation, and UDP exchange with UDP-glucose, require further investigation. Further structural elucidation of FKS1 in conjunction with substrates and inhibitors will be helpful in fully unraveling these mechanisms.

In conclusion, our study provides a comprehensive understanding of the molecular architecture and dynamic interactions within the GS complex. The identified key residues, domains, and interfaces contribute valuable insights into the regulatory mechanisms governing β-1,3-glucan biosynthesis, opening avenues for further investigations into the activation processes and potential drug targets within the FKS1-Rho1 complex.

Methods

Strain construction

Saccharomyces cerevisiae strain BY4741 was utilized for genetic manipulations. All engineered strains employed in this work are listed in Supplementary Table 2. The engineered strain BY4741-FSH was created by attaching Flag, Strep, and His tags to the C terminus of FKS1, FKS2, and FKS3, respectively, on the chromosomal locus of *S. cerevisiae* strain BY4741 using the pCas system[36,37]. For example, the Flag tag was added to FKS1 by first deleting the FKS1 gene (creating the Δfks1 strain) through co-transformation of the linear repair homologous DNA (containing the HA sequence TACCCATACGATGTTCCAGATTACGCT) with the Cas9 plasmid containing the corresponding sgRNA. All primers sequences were synthesized by Sangon Biotechnology. Then, the FKS1 gene with the attached Flag tag was integrated in situ by co-transformation of the Cas9 plasmid containing the HA gRNA with the repaired DNA. To generate FKS1 mutants, the mutant FKS1 gene was firstly cloned into plasmid pUC19, containing homologous regions to generate donor plasmid using restriction enzymes EcoRI-HF and BamHI-HF (New England Biolabs, US). The donor plasmid was introduced into *S. cerevisiae* via the LiAc/ssDNA/PEG yeast transformation method[38]. The correct clones were screened using PCR on yeast colonies with KOD FX PCR mix (Toyobo, Osaka, Japan), which were then verified by DNA sequencing. Deletions of FKS1, FKS2, FKS3 were performed using the pCas system. The target spacer was designed using the CHOPCHOP web tool (https://chopchop.cbu.uib.no/)[39]. The gene cassettes on donor plasmids were co-transformed into yeast with the corresponding Cas9 plasmid.

Cell wall isolation

Yeast cell wall isolation was performed as described previously[40]. Briefly, yeast cells were cultivated in 100 mL of YPD medium (20 g/L peptone, 10 g/L yeast extract and 20 g/L glucose) and harvested during exponential phase by centrifugation at 3600 × g for 15 min. Then, the cell pellets were resuspended in 50 mL cold deionized water and centrifuged again at 3600 × g for 15 min. Subsequently, the cell pellet was resuspended in 1 ml cold TE buffer with 1 g acid-washed glass beads. The yeast cells were broken using a mechanical bead beater setting at 50 HZ, for ten 60 s periods alternating with 50 s intervals on ice. The yeast cell wall breakage was checked by microscopic examination. The beads were spin down by a short centrifugation at 400 × g for 1 min and the supernatant was transferred into a 15 ml falcon tube. The glass beads were then washed at least six times with 1 ml buffer TE by vortex the cell suspension briefly and then spined down after each

wash at 400 × g for 1 min. All washing solution was then transferred into a 15 mL falcon tube and centrifuged at 3600 × g for 15 min. The supernatant was removed and the pellet (containing the cell wall) was resuspended in 1 ml buffer TE. This solution was transferred into 2 mL EP tubes, centrifuged again for 10 min at 10000 g. The supernatant was removed and the pellet was dried in an oven set at 110 °C overnight. The resulted cell wall fragments were stored at −20 °C until analysis.

Acidic hydrolysis and HPLC analysis of glucose-to-mannose ratio of the cell wall

The reducing sugars of the cell wall was extracted using the sulfuric acid hydrolysis method, as previously described[41]. Briefly, approximately 50 mg of cell wall fragments were collected, subjected to 375 µL 72% H_2SO_4 hydrolysis, and incubated at room temperature for 3 h. The slurry was diluted to 2 N H_2SO_4 by adding 4.75 mL of distilled water and then boiled at 100 °C for 4 h. The acidic solution was subsequently cooled and neutralized by the dropwise addition of a saturated $Ba(OH)_2$ solution, followed by overnight incubation at 4 °C. The mixture was centrifuged at 3600 × g for 20 min, and then 10 µL of the supernatant was injected for LC-RI detection. Chromatographic separation was carried out on a Bio-Rad Aminex HPX-87H column (300 × 7.8 mm). The samples were maintained at 55 °C. The flow rate was 0.5 mL/min. The HPLC mobile phase was 5 mM sulfuric acid in water. Glucose and mannose monosaccharides were used as standards and represented the glucan and mannan cell wall polysaccharides, respectively.

Protein expression and purification

FKS1. One hundred liters of yeast BY4741-FSH cells were collected by centrifugation at 1914 × g for 8 min after culturing for 16 h and resuspended in lysis buffer containing 25 mM Tris pH 8.0, 150 mM NaCl, supplemented with 1 mM phenylmethanesulfonyl fluoride (PMSF, Sigma). Subsequently, the yeast cells were homogenized under high pressure using the AH-NANO (ATS) at 1000–1100 bar, followed by centrifugation at 7656 × g for 15 min to remove the debris. The supernatant was collected and ultracentrifuged at 203,100 × g for 90 min. For membrane protein extraction, the yeast membrane was harvested and supplemented with 2.8% (w/v) n-dodecyl-β-D-maltopyranoside (DDM, Anatrace), protease inhibitors (1 mM PMSF, 0.8 µM aprotinin, 2 µM pepstatin, 5 µg/ml leupeptin), and incubated at 4 °C for 1 h. The insoluble fraction was removed by an additional centrifugation at 1812 × g for 5 min. The remaining supernatant was incubated with ANTI-FLAG M2 Affinity Gel (Sigma) at 4 °C for 30 min. The resin was rinsed with the wash buffer containing 25 mM Tris pH 8.0, 500 mM NaCl, and 0.06% (w/v) GDN (Anatrace). The FKS1 protein was eluted with the wash buffer supplemented with 0.2 mg/mL FLAG peptide. The protein was concentrated and applied to size exclusion chromatography (SEC) using a Superose 6 10/300GL column (GE Healthcare) with the SEC buffer containing 25 mM Tris pH 8.0, 150 mM NaCl, 0.06% (w/v) GDN. The peak fractions were collected and concentrated for cryo-EM sample preparation and following experiments.

Rho1. The cDNA of Rho1 was cloned from the genome of the BY4741 strain of *Saccharomyces cerevisiae* and subcloned into the pFastBac vector with the N-terminal 8 * His tag. The $Rho1^{Q68H}$ mutation were generated using a PCR-based strategy. The Bac-to-Bac baculovirus expression system (Invitrogen) was used to express the Rho1 (or $Rho1^{Q68H}$) proteins in the SF9 cells. The SF9 cells (1.8×10^6 cells/mL) were collected after 60 h of viral infection and resuspended in the lysis buffer containing 25 mM Tris pH 8.0, 150 mM NaCl. The membrane was extracted by adding 2%(w/v) DDM for 1.5 h and centrifuged at 38,759 × g for 30 min to remove the cell debris. The supernatant was loaded on Ni-NTA affinity resins (Qiagen) and rinsed with the lysis buffer supplemented with 10 mM imidazole (Sigma) and 0.02% DDM. The protein was eluted with the elution buffer containing 25 mM Tris pH 8.0, 150 mM NaCl, 0.02% (w/v) DDM, and 300 mM imidazole. The eluted protein was concentrated and applied to SEC by Superdex 200 Increase 10/300 GL column (GE Healthcare) with the SEC buffer containing 20 mM HEPES pH 7.5, 50 mM NaCl, and 0.06% (w/v) GDN.

Cross-linking of FKS1 and $Rho1^{Q68H}$

FKS1 was purified as described above, but the buffers were changed. The lysis buffer was changed to HEPES buffer. FKS1 was eluted with the elution buffer containing 20 mM HEPES pH 7.5, 100 mM NaCl, 0.06% (w/v) GDN, and concentrated to about 2.7 mg mL-1 for cross-linking. 2 mM bissulfosuccinimidyl suberate (BS3, Thermo Fisher Scientific) was added at a molar ratio of 10:1 $Rho1^{Q68H}$ to FKS1 on ice for 1 h and then quenched by 25 mM Tris at pH 8.0. The sample was applied to a Superose 6 Increase 10/300 GL column in the buffer containing 25 mM HEPES pH 7.5, 100 mM NaCl, 0.06% GDN. The peak fractions were collected and concentrated for preparation of the FKS1-$Rho1^{Q68H}$ complex cryo-EM sample.

Cryo-EM sample preparation and data acquisition

The purified protein was concentrated to ~7 mg/ml. For resting FKS1 dataset, 3.5 µL protein sample was applied to the glow-discharged (15 mA, 1 min) holey carbon grids (Quantifoil Au R1.2/1.3, 300 mesh). The grids were blotted for 2.5 s and vitrified using Vitrobot (Mark IV, Thermo Fisher Scientific) at 4° C with 100% humidity.

The grids were transferred to a 300 kV Titan Krios microscope equipped with a Gatan K2 Summit detector at Sichuan University for data collection. Defocus values of micrographs ranged from −1.1 to −1.8 µm. Each stack of 30 frames was exposed for 6 s, and the total dose of each stack was about 50 $e^-/Å^2$. The EPU program was used for data collection.

For the FKS1-Rho1 complex dataset, 4 µL protein sample was applied to the glow-discharged (15 mA, 1 min) holey carbon grids (Quantifoil Au R1.2/1.3, 300 mesh). The grids were blotted for 3.0 s and vitrified using Vitrobot at 4° C with 100% humidity and were transferred to the 300 kV Titan Krios microscope equipped with a Gatan K3 Summit detector and a GIF Quantum energy filter (slit width 20 eV) at Tsinghua University for data collection. Defocus values of micrographs ranged from −1.3 to 1.8 µm. Each movie stack was recorded for 2.56 s and the total dose of each stack was about 50 $e^-/Å^2$. The AutoEMation program was used for data collection[41]. All 32 frames in each stack were aligned and summed using the whole-image motion correction program MotionCor2 and binned to a pixel size of 1.0741 Å.

Data processing

Resting FKS1. 3799 movies were collected using the K2 Summit camera in the West China Cryo-EM Center and processed in CryoSPARC 4.1.2 (ref. 42). After motion correction and contrast transfer function (CTF) estimation, 830,031 particles were automatically picked from 3420 manually selected micrographs and were bin2 extracted[43]. After several rounds of 2D classification, the best set of particles was used to generate a map as a good reference. Two bad references were generated by manually erasing the good reference in UCSF Chimera[44]. After several rounds of heterogeneous refinement, 713,687 particles were selected, and was re-extracted with no binning using a box size of 256 pix for further 2D classification and heterogeneous refinement. 491,649 good particles were selected and imported to the 3D Variability job. The frame 0 map and the frame 19 map from class 2 were selected and then subjected to heterogeneous refinement as references. With a manually erased bad reference, 277,867 particles were selected after heterogeneous refinement and then applied to non-uniform refinement, resulting in a 3.16 Å map.

FKS1-Rho1 complex. 3456 movies were collected using the Gatan K3 Summit detector at Tsinghua University and processed in CryoSPARC 4.1.2 (ref. 42). After motion correction and CTF estimation, 1,990,283

particles were automatically picked using 2D averages generated by the FKS1 apo map as templates. The particles were bin2 extracted using a box size of 128 pix with pixel size of 2.1482 Å. After several rounds of 2D classification, ab initio reconstruction, and heterogeneous refinement, 520,005 particles were selected and subjected to local refinement, resulting in a 4.45 Å map. The particles were subjected to a Rho1-focus masked 3D classification without alignment. After two rounds of Rho1-focus masked 3D classification without alignment, 124,209 particles were applied to local refinement, resulting in a 4.45 Å additional map. This density map clearly delineates the fold of Rho1 and reveals the interaction interface with FKS1. Then the particles were unbinned re-extracted using a box size of 256 pix with pixel size of 1.087 Å. After several rounds of 2D classification and heterogeneous refinement, 93,892 particles were selected and finally subjected to local refinement, resulting in a 3.40 Å map.

Model building and refinement

The atomic coordinate of FKS1 was generated by AlphaFold2 (ref. 45). The predicted model was manually fitted to the density map in UCSF Chimera, manually rebuilt and adjusted by COOT and PHENIX[46,47].

For the FKS1-Rho1 complex, two density maps were employed for model building of the FKS1-Rho1 complex: a main map at 3.4 Å resolution and an additional map at 4.45 Å resolution. The overall structural model was built using the 4.45 Å map. The atomic coordinates for Rho1 were generated using AlphaFold2. The corrected FKS1 model and Rho1 were docked into the 4.45 Å map and manually rebuilt and adjusted using COOT and PHENIX[46,47]. Real-space refinement with secondary structure restraints was performed in PHENIX based on the 4.45 Å additional map. Given the clearer density for Rho1 in the 4.45 Å map and the excellent fit of its secondary structure, the placement of Rho1 could be confidently determined.

For detailed analysis of FKS1, we used the 3.4 Å main map, which provided increased detail in the FKS1 density, though the Rho1 density showed no significant improvement. All models were refined against the map and validated in PHENIX using the real-space refinement tool.

Pulldown assay of FKS1 and Rho1

Flag-tagged FKS1 and His-tagged Rho1 proteins (or Rho1 mutants) were purified as described above. Equal aliquots of FKS1 and Rho1 protein (or Rho1 mutant protein) were mixed at a molar ratio of ~1:10. The FKS1-Rho1 protein complex was incubated at 4 °C for 1 h in an incubation buffer containing 25 mM HEPES (pH 7.5), 100 mM NaCl, and 0.06% GDN, and 0.2 mM GTPγS or no GTP-analog. To evaluate the ability of FKS1 to bind Rho1 in the presence of GTP or GDP, 0.2 mM GTP or GDP was used to replace GTPγS in the incubation buffer. The ANTI-FLAG M2 Affinity Gel (Sigma) was added to the mixture and incubated at 4°C for 30 min. The resin was washed with the wash buffer containing 20 mM HEPES pH 7.5, 100 mM NaCl, 0.06% GDN (with 0.2 mM GTPγS/GTP/GDP or not), and the protein was eluted with the wash buffer plus 0.2 mg/mL FLAG peptide. The elute samples(IP) were analyzed by immunoblotting, the mouse anti-FLAG (1: 5000 diluted in 5% skim milk, Proteintech) and the mouse anti-HIS (1: 5000 diluted in 5% skim milk, ZenBio) were used as primary antibodies, anti-mouse IgG, HRP-linked (1: 5000 diluted in 5% skim milk, ZenBio) was used as secondary antibody.

Spot growth assay

Different FKS1 mutation strains were cultured in 5 ml YPD liquid medium at 30 °C at 220 rpm overnight and diluted with YPD liquid medium to measure OD600. The samples were gradient diluted to the OD600 was from 0.2 to 0.002. Then, 1 μl of each sample was spotted on YPD plates, which contained FK506 (1 μg/ml) or not. YPD plates were incubated at 30 °C for several days and photographed with the GeneSys. Each assay was repeated three times.

Growth curve analysis

Different FKS1 mutation strains were cultured in 5 ml YPD liquid medium at 30 °C at 220 rpm overnight and diluted with YPD liquid medium to measure OD_{600}. The OD_{600} of strains were adjusted to 0.2 and grown at 30 °C at 220 rpm. The OD_{600} was measured every 1 h until they reached their stationary phase. The experiments were repeated three times, each time with different colonies of the same strain.

FKS1 activity assay

To measure the activity of FKS1 and mutants, the wild-type FKS1 and mutants were purified and assayed using the UDP-Glo Glycosyltransferase Assay kit (Promega) to monitor UDP formation. 0.1 μM FKS1 protein was added to 25 μl of reaction mixture containing 25 mM Tris-HCl pH 8.0, 100 mM NaCl, 10% glycerol, 5 mM $MgCl_2$, 0.06% GDN, 1 μM Rho1 and 10 μM GTPγS (or 1 μM $Rho1^{Q68H}$ without GTPγS). The reaction was started by adding 400 μM UDP-Glc and was incubated at 30 °C for 1 h. The UDP detection reagent was added, and the luminescence generated was detected using a Synergy H1 Microplate Reader (BioTek).

β−1,3-glucan synthesis assay

In vitro synthesis of β−1,3-glucan assay was performed as previously described with modifications[21]. Briefly, 40 μg of purified FKS1 was added to a 2 ml reaction mixture containing 50 mM Tris-HCl pH 7.5, 33% glycerol, 0.2% CHAPS, 0.04% CHS and 20 mM KF (with 14 μg Rho1 and 4 μM GTPγS or 14 μg $Rho1^{Q68H}$). The FKS1 protein was replaced with an equal volume of FKS1 purification buffer as a control. The reaction was started by adding 2 mM UDP-Glc and was incubated at 30 °C for 40 h. Subsequently, the mixture was centrifuged at 10,000 × g for 10 min, and 100 μl of the sample collected from the bottom of the tube was transferred to a new tube. Then, 10 μl of 0.3% aniline blue was added to the 100 μl product for staining. For β-1,3-glucanase digestion, 0.2 U of β-1,3-glucanase (67138, Sigma) was added to the product and incubated at 37 °C for 30 min prior to aniline blue staining.

10 μl of each sample were placed on a glass-bottom 35-mm dish (200350, SPL Life Sciences). Imaging was performed with a FV3000 confocal microscope (Olympus Life Science) equipped with a ×60 water immersion lens. The 405 nm laser and 430–470 nm filter were used for aniline blue fluorescence.

Reporting summary

Further information on research design is available in the Nature Portfolio Reporting Summary linked to this article.

Data availability

The coordinates for the model of the FKS1 apo structure and FKS1-Rho1 complex structure in this study have been deposited in PDB under accession number 8WL6 and 8WLA, respectively. Corresponding cryo-EM density maps (including the additional map of FKS1-Rho1 complex) have been deposited in the Electron Microscopy Data Bank under accession number EMD-37612 [https://www.ebi.ac.uk/pdbe/entry/emdb/EMD37612] and EMD-37614 [https://www.ebi.ac.uk/pdbe/entry/emdb/EMD37614], respectively. A Supplementary Information file is available with this manuscript. Source data is also available with this paper as a Source Data file. Source data are provided with this paper.

References

1. Gow, N. A. R., Latge, J. P. & Munro, C. A. The fungal cell wall: structure, biosynthesis, and function. *Microbiol. Spectr.* **5**, https://doi.org/10.1128/microbiolspec.funk-0035-2016 (2017).
2. Free, S. J. Fungal cell wall organization and biosynthesis. *Adv. Genet.* **81**, 33–82 (2013).
3. Apgar, J. M. et al. Ibrexafungerp: An orally active beta-1,3-glucan synthesis inhibitor. *Bioorg. Med. Chem. Lett.* **32**, 127661 (2021).

4. Deresinski, S. C. & Stevens, D. A. Caspofungin. *Clin. Infect. Dis.* **36**, 1445–1457 (2003).
5. Lesage, G. & Bussey, H. Cell wall assembly in Saccharomyces cerevisiae. *Microbiol. Mol. Biol. Rev.* **70**, 317–343 (2006).
6. Ibe, C. & Munro, C. A. Fungal cell wall: an underexploited target for antifungal therapies. *PLoS Pathog.* **17**, e1009470 (2021).
7. Denning, D. W. Echinocandin antifungal drugs. *Lancet* **362**, 1142–1151 (2003).
8. Shematek, E. M., Braatz, J. A. & Cabib, E. Biosynthesis of the yeast cell wall. I. Preparation and properties of beta-(1 leads to 3)glucan synthetase. *J. Biol. Chem.* **255**, 888–894 (1980).
9. Shematek, E. M. & Cabib, E. Biosynthesis of the yeast cell wall. II. Regulation of beta-(1 leads to 3)glucan synthetase by ATP and GTP. *J. Biol. Chem.* **255**, 895–902 (1980).
10. Mol, P. C., Park, H. M., Mullins, J. T. & Cabib, E. A GTP-binding protein regulates the activity of (1–>3)-beta-glucan synthase, an enzyme directly involved in yeast cell wall morphogenesis. *J. Biol. Chem.* **269**, 31267–31274 (1994).
11. Kelly, R., Register, E., Hsu, M. J., Kurtz, M. & Nielsen, J. Isolation of a gene involved in 1,3-beta-glucan synthesis in Aspergillus nidulans and purification of the corresponding protein. *J. Bacteriol.* **178**, 4381–4391 (1996).
12. Mazur, P. & Baginsky, W. In vitro activity of 1,3-beta-D-glucan synthase requires the GTP-binding protein Rho1. *J. Biol. Chem.* **271**, 14604–14609 (1996).
13. Qadota, H. et al. Identification of yeast Rho1p GTPase as a regulatory subunit of 1,3-beta-glucan synthase. *Science* **272**, 279–281 (1996).
14. Drgonová, J. et al. Rho1p, a yeast protein at the interface between cell polarization and morphogenesis. *Science* **272**, 277–279 (1996).
15. Douglas, C. M. et al. The Saccharomyces cerevisiae FKS1 (ETG1) gene encodes an integral membrane protein which is a subunit of 1,3-beta-D-glucan synthase. *Proc. Natl Acad. Sci. USA* **91**, 12907–12911 (1994).
16. Douglas, C. M. et al. Identification of the FKS1 gene of Candida albicans as the essential target of 1,3-beta-D-glucan synthase inhibitors. *Antimicrob. Agents Chemother.* **41**, 2471–2479 (1997).
17. Wang, J. et al. The FKS family genes cause changes in cell wall morphology resulted in regulation of anti-autolytic ability in Saccharomyces cerevisiae. *Bioresour. Technol.* **249**, 49–56 (2018).
18. Dijkgraaf, G. J., Abe, M., Ohya, Y. & Bussey, H. Mutations in Fks1p affect the cell wall content of beta-1,3- and beta-1,6-glucan in Saccharomyces cerevisiae. *Yeast* **19**, 671–690 (2002).
19. Mazur, P. et al. Differential expression and function of two homologous subunits of yeast 1,3-beta-D-glucan synthase. *Mol. Cell. Biol.* **15**, 5671–5681 (1995).
20. Katiyar, S. K. et al. Fks1 and Fks2 are functionally redundant but differentially regulated in Candida glabrata: implications for echinocandin resistance. *Antimicrob. Agents Chemother.* **56**, 6304–6309 (2012).
21. Hu, X. et al. Structural and mechanistic insights into fungal beta-1,3-glucan synthase FKS1. *Nature* **616**, 190–198 (2023).
22. Zhao, C. R. et al. Structure of a fungal 1,3-beta-glucan synthase. *Sci. Adv.* **9**, eadh7820 (2023).
23. Holm, L. & Laakso, L. M. Dali server update. *Nucleic Acids Res.* **44**, W351–W355 (2016).
24. van Kempen, M. et al. Fast and accurate protein structure search with Foldseek. *Nat. Biotechnol.* **42**, 243–246 (2023).
25. Morgan, J. L., Strumillo, J. & Zimmer, J. Crystallographic snapshot of cellulose synthesis and membrane translocation. *Nature* **493**, 181–186 (2013).
26. Morgan, J. L., McNamara, J. T. & Zimmer, J. Mechanism of activation of bacterial cellulose synthase by cyclic di-GMP. *Nat. Struct. Mol. Biol.* **21**, 489–496 (2014).
27. Morgan, J. L. et al. Observing cellulose biosynthesis and membrane translocation in crystallo. *Nature* **531**, 329–334 (2016).
28. Krissinel, E. & Henrick, K. Inference of macromolecular assemblies from crystalline state. *J. Mol. Biol.* **372**, 774–797 (2007).
29. Johnson, M. E. & Edlind, T. D. Topological and mutational analysis of Saccharomyces cerevisiae Fks1. *Eukaryot. Cell* **11**, 952–960 (2012).
30. Cabib, E., Drgonova, J. & Drgon, T. Role of small G proteins in yeast cell polarization and wall biosynthesis. *Annu. Rev. Biochem.* **67**, 307–333 (1998).
31. Wagener, J., Striegler, K. & Wagener, N. alpha- and beta-1,3-glucan synthesis and remodeling. *Curr. Top. Microbiol. Immunol.* **425**, 53–82 (2020).
32. Vetter, I. R. & Wittinghofer, A. The guanine nucleotide-binding switch in three dimensions. *Science* **294**, 1299–1304 (2001).
33. Yamashita, M. et al. Structural basis for the Rho- and phosphoinositide-dependent localization of the exocyst subunit Sec3. *Nat. Struct. Mol. Biol.* **17**, 180–186 (2010).
34. Qadota, H., Anraku, Y., Botstein, D. & Ohya, Y. Conditional lethality of a yeast strain expressing human RHOA in place of RHO1. *Proc. Natl. Acad. Sci. USA.* **91**, 9317–9321 (1994).
35. Inoue, S. B., Qadota, H., Arisawa, M., Watanabe, T. & Ohya, Y. Prenylation of Rho1p is required for activation of yeast 1, 3-beta-glucan synthase. *J. Biol. Chem.* **274**, 38119–38124 (1999).
36. Funakoshi, M. & Hochstrasser, M. Small epitope-linker modules for PCR-based C-terminal tagging in Saccharomyces cerevisiae. *Yeast* **26**, 185–192 (2009).
37. Ryan, O. W. et al. Selection of chromosomal DNA libraries using a multiplex CRISPR system. *Elife* **3**, e03703 (2014).
38. Gietz, R. D. & Schiestl, R. H. High-efficiency yeast transformation using the LiAc/SS carrier DNA/PEG method. *Nat. Protoc.* **2**, 31–34 (2007).
39. Labun, K., Montague, T. G., Gagnon, J. A., Thyme, S. B. & Valen, E. CHOPCHOP v2: a web tool for the next generation of CRISPR genome engineering. *Nucleic Acids Res.* **44**, W272–276, (2016).
40. Francois, J. M. A simple method for quantitative determination of polysaccharides in fungal cell walls. *Nat. Protoc.* **1**, 2995–3000 (2006).
41. Lei, J. & Frank, J. Automated acquisition of cryo-electron micrographs for single particle reconstruction on an FEI Tecnai electron microscope. *J. Struct. Biol.* **150**, 69–80 (2005).
42. Punjani, A., Rubinstein, J. L., Fleet, D. J. & Brubaker, M. A. cryoSPARC: algorithms for rapid unsupervised cryo-EM structure determination. *Nat. Methods* **14**, 290 (2017).
43. Zheng, S. Q. et al. MotionCor2: anisotropic correction of beam-induced motion for improved cryo-electron microscopy. *Nat. Methods* **14**, 331–332 (2017).
44. Pettersen, E. F. et al. UCSF chimeraX: structure visualization for researchers, educators, and developers. *Protein Sci.* **30**, 70–82 (2021).
45. Jumper, J. et al. Highly accurate protein structure prediction with AlphaFold. *Nature* **596**, 583–589 (2021).
46. Adams, P. D. et al. PHENIX: a comprehensive python-based system for macromolecular structure solution. *Acta Crystallogr. D Biol. Crystallogr.* **66**, 213–221 (2010).
47. Emsley, P., Lohkamp, B., Scott, W. G. & Cowtan, K. Features and development of coot. *Acta Crystallogr. D Biol. Crystallogr.* **66**, 486–501 (2010).

Acknowledgements

We thank SKLB West China Cryo-EM Center in Sichuan University for assistance in cryo-EM data collection. We thank Ping Yin for critical comments on the manuscript. This work was financially supported by the National Key R&D Program of China (2023YFC3503903 and 2023YFC3503902), the National Natural Science Foundation of China

(32471264 X.W.; 32471492 Y.Z. L.), the Haihe Laboratory of Sustainable Chemical Transformations for financial support (24HHWCSS00006), and the Key-Area Research and Development Program of Guangdong Province (2020B0303070002). This work was supported in part by the Sichuan Province Innovative Talent Funding Project for Postdoctoral Fellows to Jialu Li.

Author contributions

X.W., D.D., and Y.Z.L. designed the experiments. J.L.L., H.Y.L., J.X.L., X.L.D., and W.Y.Q. expressed, purified the FKS1 protein. H.Y.L., H.H.L., and J.L. constructed all yeast strains used in the article. J.L.L., Q.J.X., A.Q.Z., and C.Y.Y. analyzed the cryo-EM data and built the model. J.L.L., J.L., H.Y.L., and X.W. performed the biochemical assay. X.W. and D.D. contributed to the initial drafting of the manuscript. Y.Z.L., C.Y.Y., and L.G. provided critical discussions and revisions of the manuscript content.

Competing interests

The authors declare no competing interests.

Additional information

Supplementary information The online version contains supplementary material available at https://doi.org/10.1038/s41467-025-57152-7.

Correspondence and requests for materials should be addressed to Dong Deng, Yunzi Luo or Xiang Wang.

Peer review information *Nature Communications* thanks Jochen Zimmer and the other anonymous reviewer(s) for their contribution to the peer review of this work. A peer review file is available.